ISPRS Journal of Photogrammetry and Remote Sensing 84 (2013) 12–22

Contents lists available at SciVerse ScienceDirect

ISPRS Journal of Photogrammetry and Remote Sensing

journal homepage: www.elsevier.com/locate/isprsjprs

Uncertainty analysis of remote sensing of colored dissolved organic matter: Evaluations and comparisons for three rivers in North America

Weining Zhu [a,b,*], Qian Yu [c], Yong Q. Tian [a,b]

[a] Institute for Great Lakes Research, Central Michigan University, United States
[b] Department of Geography, Central Michigan University, United States
[c] Department of Geosciences, University of Massachusetts Amherst, United States

ARTICLE INFO

Article history:
Received 10 May 2013
Received in revised form 2 July 2013
Accepted 5 July 2013

Keywords:
Uncertainty analysis
Remote sensing inversion
CDOM
River systems
EO-1 Hyperion
QAA-CDOM

ABSTRACT

The uncertainties involved in remote sensing inversion of CDOM (Colored Dissolved Organic Matter) were analyzed in estuarine and coastal regions of three North American rivers: Mississippi, Hudson, and Neponset. Water optical and biogeochemical properties, including CDOM absorption and above-surface spectra, were collected in very high resolution. CDOM's concentrations ($a_g(440)$, absorption coefficient at 440 nm) were inverted from EO-1 Hyperion images, using a quasi-analytical algorithm for CDOM (QAA-CDOM). Uncertainties are classified to five levels, in which the underwater measurement uncertainty (level 1), image preprocessing uncertainty (level 4) and inverse model uncertainty (level 5) were evaluated. Results indicate that at level 1, in situ CDOM measurement is significant with 0.1 in the unit of QSU and 0.01 in the unit of $a_g(440)$ (m^{-1}). At level 4, surface wave is a potential uncertainty source for high-resolution images in estuarine and coastal regions. The remote sensing reflectance of wavy water is about 10 times of the truth. At level 5, the overall uncertainty of QAA-CDOM inversion is 0.006 m^{-1}, with accuracy $R^2 = 0.77$, $k = 1.1$ and $RMSE_{log} = 0.33$ m^{-1}. The correlations between uncertainties and other water properties indicate that the large uncertainty in some rivers, such as the Neponset and Atchafalaya, might be caused by high-concentration chlorophyll or sediments. The relationships among the three level uncertainties show that the level 1 uncertainty generally does not propagate into level 4 and 5, but the large uncertainty at level 4 usually introduce large uncertainty at level 5.

Published by Elsevier B.V. on behalf of International Society for Photogrammetry and Remote Sensing, Inc. (ISPRS).

1. Introduction

Colored dissolved organic matter (CDOM) is the optically measurable component of dissolved organic matter in water. CDOM in nature mostly come from decaying vegetation detritus and also sometimes related to anthropogenic releasing (Bukata et al., 1995; Nelson and Siegel, 2002). Knowing CDOM concentration and distribution in riverine, estuarine and coastal regions has important implications to both terrestrial and aquatic ecosystems, such as tracing dissolved organic carbon (DOC) (Chen et al., 2004; Ferrari et al., 1996; Stedmon et al., 2006; Vodacek et al., 1997), monitoring water quality and aquatic photosynthesis (Bukata et al., 1995; Kirk, 1994), and assessing terrestrial carbon transportation to coastal water (Blough et al., 1993; Del Castillo et al., 1999; Nelson et al., 2010).

Remote sensing provides a feasible approach to assess CDOM at large spatial scale. However, compared with the other two major ocean-color components, chlorophyll (CHL) and non-algal particles (NAPs), the remote sensing inversion of CDOM is not fully investigated. Large uncertainties are remained in many aspects of CDOM inversion, especially for complex waters in estuarine and coastal regions. (1) The uncertainty of field CDOM measurement. Small sampling size and narrow CDOM range usually limit algorithm validations and uncertainty assessments. Several recent published studies have used a few to a dozen in situ discrete samples to validate the inversion results without uncertainty analysis (Brando and Dekker, 2003; Ortega-Retuerta et al., 2010). In addition, most of previous estuarine and coastal CDOM studies and their validations were carried out in the sites where the spatial variation of CDOM is limited. Therefore the algorithms, parameters, coefficients, as well as the uncertainty assessment concluded from one site could be inappropriate and hence produce large uncertainties when transferring to other sites. (2) The uncertainty of satellite imagery. High spatial resolution images in estuarine and coastal regions contain more spatial variation and uncertainties than those coarse images for open sea ocean color studies (e.g., 1 km for SeaWiFS and MODIS) (Carder et al., 1999; Garver and Siegel, 1997; O'Reilly et al., 1998; Siegel et al., 2002). Because of

* Corresponding author at: Department of Geography, Central Michigan University, United States. Tel.: +1 989 774 7697.
E-mail address: zhu3w@cmich.edu (W. Zhu).

0924-2716/$ - see front matter Published by Elsevier B.V. on behalf of International Society for Photogrammetry and Remote Sensing, Inc. (ISPRS).
http://dx.doi.org/10.1016/j.isprsjprs.2013.07.005

complicated freshwater and marine mixing environment, the possible uncertainty sources include the wind-driven glints, boat-driven whitecaps, and anthropogenic release, etc., which arise more often in estuarine and coastal regions than in open sea. These uncertainties usually vary in relatively small space and hence are unseen from low resolution images due to mixed pixels, but they will be revealed by high-resolution images and hence bring interferences and new challenges for ocean-color remote sensing inversion. (3) The uncertainty of CDOM algorithm. Inversion algorithms have not been well developed for CDOM, particularly for complex riverine and coastal waters. Most of previous algorithms are in empirical or oriented to simple CDOM-poor waters in open sea, where CDOM is often taken as the by-products of phytoplankton and sediments are generally in low concentration (O'Reilly et al., 1998; Sathyendranath et al., 1994). When these simple algorithms are applied to complex CDOM-rich waters in estuaries and coasts, where CDOM, CHL and sediments are all independent and likely in high concentration, they tend to bring considerable uncertainties (Yu et al., 2010; Zhu et al., 2011). Therefore it is really necessary to design new algorithms and evaluate their uncertainty for complex waters.

In fact, remote sensing inversion of CDOM in estuarine and coastal regions is extremely complicated. Uncertainties will be generated, propagated, and accumulated in the processes of in situ measurement, acquisition and preprocessing of satellite images, and all steps of inverse algorithms. The former uncertainty analyses of remote sensing inversion of ocean color components often focused on one level (Antoine et al., 2008; Lee et al., 2010; Melin, 2010; Wang et al., 2005). For example, Antoine et al. (2008) discussed the uncertainties introduced by satellite sensors, and Lee et al. (2010) discussed the uncertainties induced by QAA algorithm. In our study, we suggest classifying CDOM inversion uncertainty to five levels according to their order, including underwater measurement uncertainty (level 1), above-surface measurement uncertainty (level 2), satellite measurement uncertainty (level 3), image preprocessing uncertainty (level 4), and inverse model uncertainty (level 5) (Fig. 1). The level 1 is the uncertainty of measured CDOM concentration via conventional underwater optical instruments, such as a fluorometer or spectrophotometer. Actually any instrumental measurement will introduce uncertainties depending on random noise, instrumental calibration errors, and instrumental accuracy, etc. As far as we know, there are no studies on the uncertainty analysis of in situ CDOM measurements. Both level 2 and 3 uncertainties are related to spectral measurements. Level 2 is the uncertainty of above-surface spectral measurement of water. All in-water components, CDOM, chlorophyll, non-algal particles, and water conditions, such as surface wave and white caps, will contribute the above-surface spectrum uncertainties. Level 3 is the uncertainty of satellite spectral response, similar to the level 2 but adding the atmospheric effect. Level 4 and 5 are model uncertainties. Level 4 is the uncertainty contained in the input data to inverse models, e.g., remote sensing reflectance. This uncertainty is generated by satellite images preprocessing, such as atmospheric correction and water surface reflectance removal. The uncertainty in level 5 is generated by the inversion model itself. Level 4 and 5 uncertainties are often known as the errors between the model-derived estimates and the ground truth. Moreover, these 5-level uncertainties are not fully independent of each other – uncertainties at low levels may propagate to high levels.

The objective of this study is to evaluate the uncertainties involved in the whole process of remote sensing inversion of CDOM for estuarine and coastal waters, using our best solutions (high-resolution field measurements, high-resolution images, and high accuracy algorithm). We focused on the evaluation of uncertainties on the level 1, 4 and 5. These evaluations were based on recent data acquired from three rivers: the Mississippi, Hudson and Neponset, as well as their adjacent sites. We will evaluate level 1 uncertainties by analyzing the in situ data, the level 4 uncertainties by comparing satellite acquired (after atmospheric corrections) and the field measured spectra, and level 5 uncertainties by comparing the model derived and field measured CDOM concentrations. The impacts of low level uncertainties on the high levels will be discussed in the last section.

2. Data collections and processing

2.1. Study sites

Our study sites locate in estuarine regions of three river systems in U.S. – the Mississippi site (including Atchafalaya River, Mississippi River and their plumes, and the Northern Gulf of Mexico), the Hudson site (including the Hackensack River, Passaic River, Newark Bay, Upper/Lower New York Bay, Raritan River, Raritan Bay, and Hudson River), and the Neponset Site (including the Neponset River and Dorchester Bay), see Fig. 2. The Mississippi River, with length 3730 km, is the longest river and has the largest drainage basin in the North America, and the length of the Hudson River and Neponset River are 507 km and 47 km, respectively. Due to the large discharge and massive sediment transportation, the Mississippi and Atchafalaya estuaries show large sediment plumes. The estuaries of Hudson and Neponset are adjacent to highly urbanized areas, New York City and Boston, respectively. In this study we use the three rivers as the representatives of river systems at different scale – large, medium, and small. They locate in different climate zones: the Mississippi and Atchafalaya estuaries are in sub-tropical region and the Hudson and Neponset are in temperate region with high seasonal variations.

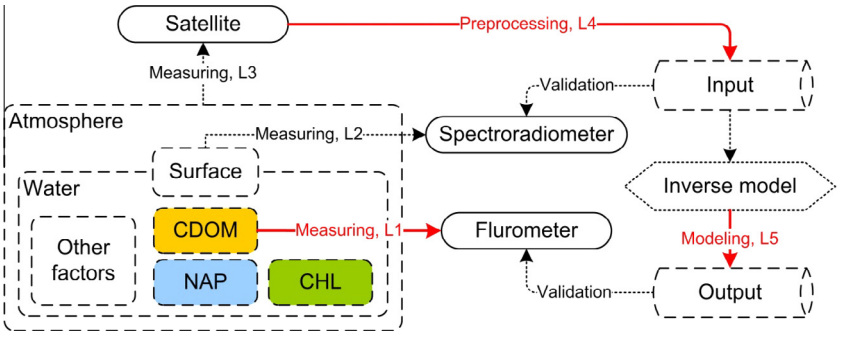

Fig. 1. Uncertainties and their levels remote sensing inversion of CDOM. The first 3 levels are related to the field measurements of CDOM, reflectance above water surface and at the top of atmosphere. Each factor contained in the dashed box contributes the major uncertainties measured by the corresponding instrument.

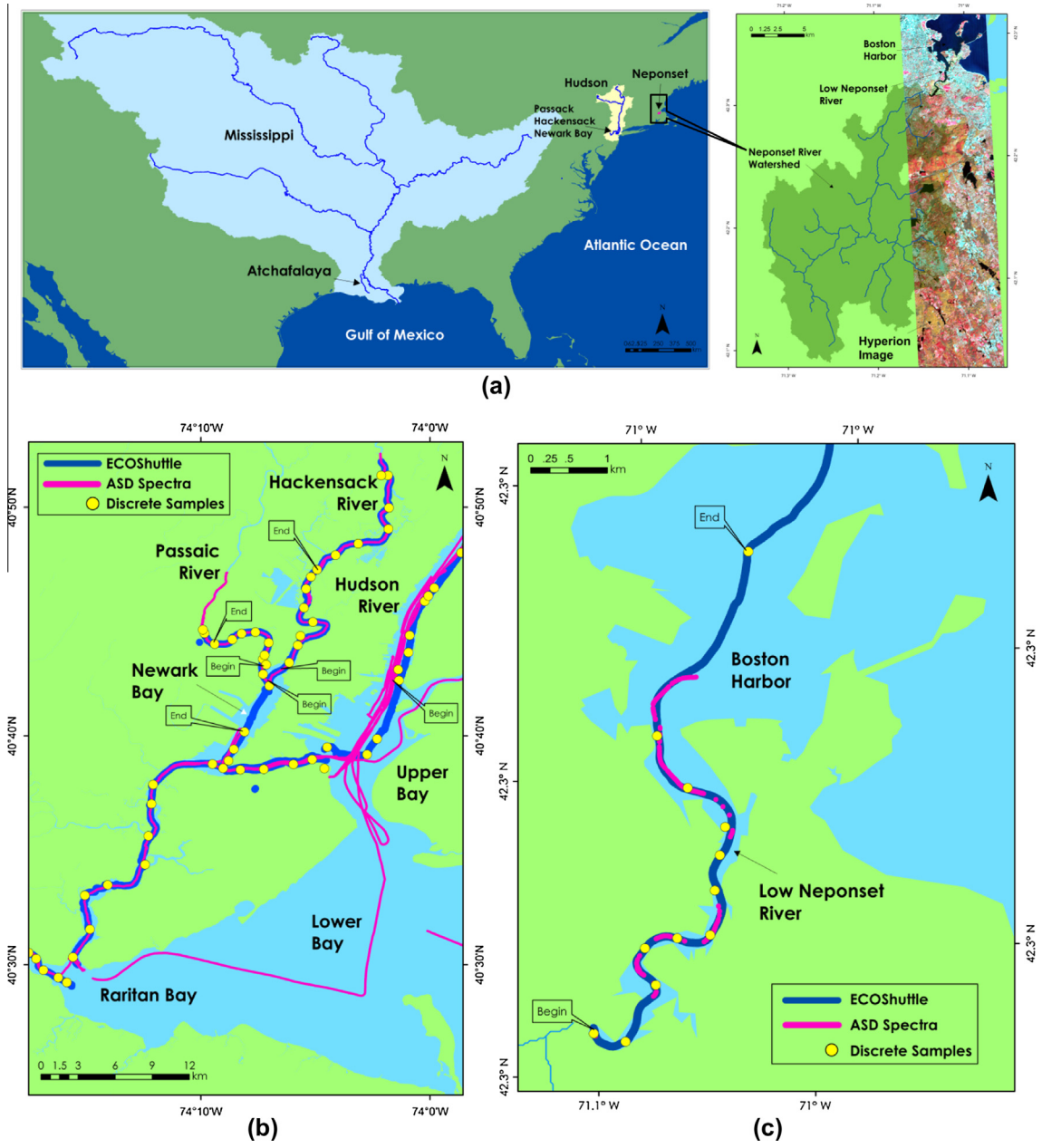

Fig. 2. Maps of three study sites, including watersheds, main rivers, cruise tracks (ECOShuttle), discrete sampling locations, above-surface spectrum locations (ASD), and EO-1 Hyperion scenes. (a) Watersheds and Rivers' main channels; One Hyperion image (11/04/2009) acquired in the Neponset watershed (b) 2006 and 2010 Cruises in Hudson Site; (c) 2009 Cruise in Neponset Site. Refer to (Zhu et al., 2011) for the 2007 cruise map in Mississippi site and other images. Data between 'Begin' and 'End' tags were used to analyze level 5 uncertainties. The end point (not shown) of Hudson River is upper away from the begin point about 55 km.

2.2. Field measurements and image acquisition

We have conducted a number of field measurements in the three rivers in the past 5 years. Generally there are three types of in situ measurements: underwater measurements by ECOShuttle or Mini-Shuttle, discrete sample measurements by conventional instruments carried out in shipboard or land Labs, and above-surface spectral measurements by spectrometers. The ECOShuttle is a towed, undulating vehicle based on the Nu-Shuttle manufactured by Chelsea Instruments. It carries instrumental sensors for measuring a number of water properties – depth, temperature, salinity, attenuation and absorption coefficients (by AC-9), CDOM, CHL, OBS (Optical Backscattering), zooplankton, etc. CDOM is measured by a SeaTech CDOM fluorometer. The Mini-Shuttle, usually used in small rivers or shallow water in short cruises, is similar to ECOShuttle but with fewer sensors mounted. ECO/Mini-Shuttle is capable of measuring with very high frequency (~0.3 s) and hence acquiring a very high resolution dataset for each above water property. The discrete samplings during cruises were conducted concurrently with the ECO/Mini-Shuttle's measurements at about 10–30 min interval, and then the bottled samples were analyzed in labs for CDOM calibration and DOC measurement. A spectroradiometer (ASD FieldSpec® 3) was used to measure water above-surface reflectance, upwelling radiance, and sky radiance. Water spectra (350–2500 nm, 1 nm interval) were measured with high frequency (~10 s–2 min). To derive the remote sensing reflectance, the downwelling irradiance was also measured by an Ocean Optics® Jaz spectrometer module in company with the ASD measurement. The date, instrumentation, and sampling number of each cruise used in this study are listed in the Table 1. More

details of field measurements can be referred to our previous works (Chen, 1999; Chen and Gardner, 2004; Gardner et al., 2005; Huang and Chen, 2009; Zhu et al., 2011).

In this study we used satellite images acquired by EO-1 Hyperion. Hyperion provides hyperspectral imagery capable of resolving 220 spectral bands (from 0.4 to 2.5 μm) with 10 nm bandwidth at 30 m spatial resolution. Both spatial and spectral resolutions are suitable for remote sensing inversion in estuarine and coastal regions, where river channels could be as narrow as a few 100 m wide and waters are fairly complicated and highly varied. The Hyperion images were requested to cover the three study sites and best available to match the field measurement time for each cruise (see Table 1 and an example shown in Fig. 2). Some past images were also retrieved from USGS archives. Most of these images are cloud free. A few partly cloudy images were used if water bodies are cloud free.

2.3. Data calibration and preprocessing

ECO/Mini-Shuttle sensors measure each ocean color component (CDOM, CHL and NAP) in voltage. Relationships between voltage (V) and each concentration unit (CDOM: QSU, CHL: mg/m^3, and NAP: FTU) are known as good linear correlations (Chen, 1999; Chen and Gardner, 2004; Gardner et al., 2005; Huang and Chen, 2009). For example, in Mississippi site, they can be converted to QSU, mg/m^3, and FTU by $QSU = 30V_{cdom}$, mg/m^3 = $10V_{chl}$, and $FTU = 500V_{obs}$, respectively. While in ocean color science, the absorption coefficient of CDOM at 440 nm, $a_g(440)$, is often taken as the indicator of CDOM concentration. The fluorescent intensity of CDOM needs to be converted to $a_g(440)$ for parameter calibration and result validation. Similarly, the conversion of CHL and NAP are also necessary if we want to compare them with CDOM and to know their contributions to water's total absorption coefficients (directly measured by AC-9). In this study, we used the following relationships to make the conversion.

(1) According to all in situ discrete sample data measured in our three sites, relationship between CDOM QSU and $a_g(440)$ is formulated as:

$$a_g(440) = 0.122 \times [\mathrm{QSU}]^{0.464} \quad (1)$$

(2) According to Bricaud et al. (1995), relationship between chlorophyll's concentration mg/m^3 and $a_{ph}(440)$ is formulated as:

$$a_{ph}(440) = 0.0403 \times [\mathrm{mg/m^3}]^{0.668} \quad (2)$$

(3) Given the above two relationships, according to AC-9 and OBS data continuously measured by ECOShuttle, relationship between sediment concentration (FTU) and $a_d(440)$ (m^{-1}) is set by

$$a_d(440) = 0.018 \times [\mathrm{FTU}] \quad (3)$$

Hyperion Level 1G images went through a long and complicated preprocessing including detector correction (replacing the missing lines, destriping, denoising), atmospheric correction, water surface reflectance removal, and required bands calculation for inverse algorithms. Eventually we obtain the remote sensing reflectance (R_{rs}) as the input data. The details of in situ data conversion and image preprocessing can be referred to (Zhu et al., 2011) and (Zhu and Yu, in press).

3. Methods

3.1. Evaluation of uncertainty

In a science and engineering notation, uncertainty means the difference between a numerical value that we obtained and that it actually should be. Sometimes it is also called the error between the measurement and the truth. Physically we are unable to obtain the actual truth but always obtain the results returned by instruments or techniques used to make the measurements. Therefore the truth and hence the uncertainty can be evaluated by statistical analysis of a number of measurements. According to the Joint Committee for Guides in Metrology of BIMP (Bureau International des Poids et Mesures), there are two types of uncertainty, type A and type B. The type A standard uncertainty can be calculated by

$$u_A = \sqrt{\frac{\sum_{i=1}^{n}(x_i - \bar{x})^2}{n(n-1)}} \quad (4)$$

where $\bar{x}$ is the expectation (arithmetic mean or average) of a quantity x (JCGM, 2008) and n is the sample size, i.e., the number of observations. Evaluation of Type A uncertainty requires that the measurements are repeatable, that is, measurement should be conducted in the same conditions and the same object. The Type B evaluation of standard uncertainty is based on other knowledge rather than the statistics. Although there is not always a simple correspondence, Type A and Type B uncertainties can be thought as the random and systematic errors, respectively. To evaluate the relationship between the standard uncertainty and x itself, the normalized uncertainty is calculated by

$$u_{A1} = \frac{u_A}{\bar{x}} \quad (5)$$

The above uncertainty quantifications for measurement can be similarly applied to model uncertainty of remote sensing inversions. Comparing the estimated value from inversion with in situ measure, we can calculate model uncertainty of inversion algorithms.

$$u_A = \sqrt{\frac{\sum_{i=1}^{n}(x_i^{derived} - x_i^{measured})^2}{n(n-1)}} \quad (6)$$

With respect to the real measurements that are generally distributed around the true value within a specific range, there is another type of normalized uncertainty expressed by

$$u_{A2} = \frac{u_A}{max(x_{measured}) - min(x_{measured})} \quad (7)$$

The expressions of other normal statistical variables for uncertainty related quantification, such as the error, absolute mean error, absolute mean error percentage, $\mathrm{error_{log}}$, SD (Standard Deviation), RMSE, $\mathrm{RMSE_{log}}$, can be referred to IOCCG (2006) and

Table 1
Cruise date and the amount of raw water samples collected in each cruise, and EO-1 Hyperion images acquired around the cruise date (in the same year of each cruise).

Cruise, year	Instruments	Date	Shuttle	Discrete	Spectral	Hyperion date
Hudson, 2006	ASD, ECOShuttle	10/23–10/25	230,000	~40	2900	09/07/2004, 12/3
Mississippi, 2007	ASD, ECOShuttle	08/24–08/31	1,000,000	150	20,000	08/27, 09/04
Neponset, 2009	ASD, MiniShuttle	09/25, 11/04	45,000	25	1500	11/04
Hudson, 2010	ASD, JAZ, ECOShuttle	07/28–08/07	1,000,000	~150	19,000	07/31, 09/02, 10/06

Zhu et al. (2011). It is worth to mention that the Eqs. 4 and 6 can be expressed by $SD/n^{0.5}$ and $RMSE/n^{0.5}$, indicating that the uncertainty is highly related to sampling size.

3.2. Qaa-cdom

In this study, the QAA-CDOM algorithm (Zhu and Yu, in press) was employed to estimate CDOM concentration $a_g(440)$. QAA-CDOM was developed based on Lee's QAA algorithm (Lee et al., 2002, 2007) and its extension, QAA-E by our earlier research (Zhu et al., 2011). QAA is a quasi-analytical level-by-level algorithm combining a series of empirical, semi-analytical, and analytical algorithms. In QAA, only R_{rs} at several wavelengths (410, 440, 490, 555, and 640 nm) is required as input data, and at multiple levels, the algorithm outputs r_{rs}, absorption and backscattering coefficients of water (a_t, b_{bp}) (total), chlorophyll (a_{ph}, b_{ph}) and CDM (a_{dg}, b_d) (CDOM and NAP together) for the four wavelengths. QAA has been tested and applied in many studies (Chang and Gould, 2006; Le et al., 2009; Lee and Carder, 2004; Zhan et al., 2005). QAA's output $a_{dg}(440)$, however, has been proven to be too rough to represent $a_g(440)$ in estuarine and coastal turbid waters (Zhu et al., 2011). Therefore, QAA's extension, QAA-E, was developed, in which $a_g(440)$ is exactly derived using either a_d-based or a_g-based methods. Recently, QAA-E has been further improved to QAA-CDOM (Zhu and Yu, in press) in which a QAA's original function and a few parameters have been optimized by integrating synthetic data, high spatial resolution in situ data from our Mississippi cruise, and NASA bio-Optical Marine Algorithm Dataset (NOMAD) collected globally during the last decades. QAA-CDOM was validated for excellent inversion accuracy (<25%) and being suitable for a wide range of CDOM variation (0.01–13.3 m^{-1}). Recently it also has been successfully applied to estimate CDOM distributions and dynamics in estuarine and coastal regions of 10 global major rivers by using EO-1 Hyperion imagery (Zhu et al., 2013).

4. Results and discussion

The following will evaluate the uncertainty contained in field CDOM measurements (level 1), satellite images preprocessing (level 4) and remote sensing inversion models (level 5) respectively. We will also discuss the possible reasons of uncertainty at level 5 and show if uncertainties are propagated between different levels.

4.1. Uncertainty of in situ measurements

The best way to assess the measurement uncertainty is to statistically evaluate repetitive measurement. Because it is difficult to use moving ECO/Mini-Shuttles to implement a rigorous repetitive measurement, we used multiple measurements, which were taken in adjacent space and consecutive time along the cruise, to represent the repetitive samples for uncertainty assessment. We assume within a very small extent, water is well mixed and the water properties are generally unchanged. This assumption is valid because ECO/Mini-Shuttles can take near-continuous measurements in very short sampling interval (~0.2–0.3 s).

We first need to determine in what extent water can be regarded as the 'same'. Due to stratification, vertical variations of ocean color components along water depth z are more significant compared with the horizontal variations, namely, in the x and y directions. Therefore when we set the extent of the 'same' water, the range of z is much smaller than x and y, making the water volume as a very thin layer. Here we use the distance d along cruise tracks to represent horizontal dimension as a substitute for the x and y pair. For instance, d = 10 m and z = 1.35–1.45 m represent the water samples within a 10 m distance along the track and water depth from 1.35 to 1.45 m. Fig. 3 shows the sampling profile along the Neponset cruise track. In a very small space (10 m × 0.1 m), MiniShuttle measured 11 samples, illustrated in the zoom-in window.

We then selected 10 datasets from three study sites for assessing measurement uncertainty. Each dataset contains sufficient water samples (no less than 10) in a spatial extent as small as possible, particularly constrained in a thin water layer to minimize the stratification effect. These selected datasets all passed a normal distribution test, the widely-used Shapiro–Wilk test, to guarantee they contain random uncertainty only. As the suggestion given by the Shapiro–Wilk test, if $p > 0.05$, we cannot reject the null hypothesis that the tested samples are normally distributed. The results (Table 2) indicate that each dataset is likely from a normal distribution. These guaranteed observations in each dataset did not cross thin layer and stratification effect was little. We also tested the correlations between the sampling depth and CDOM concentration to confirm the water is well-mixed. The results show that except the Neponset and Boston Bay datasets, others do not show strong correlations. Nevertheless, we still keep the two Neponset datasets for comparison with other sites.

The average uncertainty for all 10 datasets, calculated by the Eq. (4), is 0.00288 volts. If we convert it to QSU by multiplying 30, we get 0.086 QSU. This value, closing to 0.1 QSU, implies that in the unit of QSU, underwater CDOM measurement is accurate to the tenths place. If we further convert it to absorption coefficient using Eq. (1), we obtained that the uncertainty of $a_g(440)$ is 0.039 m^{-1}. Similarly, it indicates that absorption coefficient is accurate to the hundredths place. If we use normalized uncertainty given by Eq. (5), then this uncertainty will be independent of unit. In this study, the average normalized uncertainty of 10 datasets is 0.26%, indicating that the measures of CDOM in situ concentration are subject to 0.26% uncertainty. If we exclude the Neponset data, then the uncertainties measured in volts, QSU, and absorption coefficient are 0.00067, 0.02 and 0.019, respectively, and their normalized uncertainty is 0.11%. The above uncertainties are sourced from in situ CDOM measurements in volts using fluorometer. Other instruments and different measuring conditions, such as using conventional spectrophotometers in labs, may result in different uncertainty magnitude. For example, photometric accuracies of Cary-60 and DU-800 spectrophotometers are both ±0.005 Abs, which equals absorption coefficient ±1.15 m^{-1} if using 10 mm cuvette. This instrument uncertainty may lead to large normalized uncertainty if measuring very low-CDOM waters. Nevertheless, we do think above resultant uncertainties are representative for real-time in situ CDOM measurement using fluorescent property.

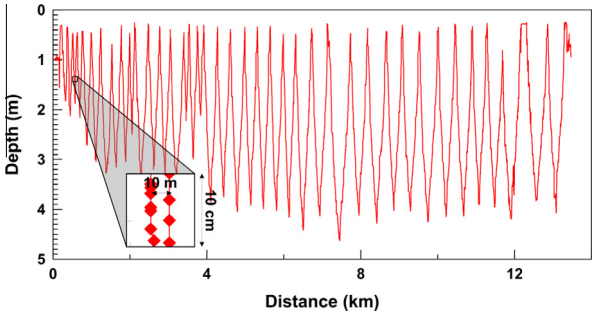

Fig. 3. The ECOShuttle (MiniShuttle) track profile underwater, in the Neponset site. The zoom-in window shows an example that when the shuttle was moved up (the left column) and down (the right column), about 11 samples were measured, within a 10 m * 10 cm space.

Table 2
CDOM measurement uncertainties (level 1) of 10 datasets over three study sites. Data were measured from a space $d \times \Delta z$, where d and z are sampling distance and depth, respectively, see Fig. 3. For distances in Hudson regions (set 1–5), distance is so short that GPS cannot measure. n is sample size, p is the probability of normality given by Shapiro–Wilk test, R is the correlation coefficient between depth and CDOM.

Set#	Location	d (m)	z (m)		n	p	CDOM (V)			R	U_A	U_{A1}
			Max	Min			Max	Min	Mean			
1	Hudson	<0.1	4.84	4.82	18	0.11	0.7399	0.7277	0.7350	−0.33	7.93E−4	1.08E−3
2	Passaic	<0.1	0.73	0.62	39	0.09	2.0855	2.0708	2.0801	0.20	5.61E−4	2.70E−4
3	Hackensack	<0.1	0.98	0.79	38	0.05	1.7680	1.7534	1.7608	0.55	6.27E−4	3.56E−4
4	Raritan	<0.1	1.00	0.91	38	0.06	1.0586	1.0073	1.0486	−0.32	1.27E−3	1.21E−3
5	Newark Bay	<0.1	0.87	0.68	28	0.07	1.0622	1.0537	1.0584	0.40	4.20E−4	3.97E−4
6	Neponset	29	24.52	20.15	27	0.12	1.6654	1.2894	1.4690	−0.84	2.27E−2	1.55E−2
7	Boston Bay	76	4.12	3.14	11	0.31	0.3594	0.3455	0.3531	−0.94	1.53E−3	4.33E−3
8	Mississippi	51	0.21	0.17	11	0.07	1.1856	1.1815	1.1841	0.39	4.52E−4	3.82E−4
9	Atchafalaya	100	1.64	1.34	25	0.73	0.1893	0.1864	0.1878	0.14	1.53E−4	8.13E−4
10	Gulf of Mexico	142	26.5	22.7	20	0.10	0.1449	0.1383	0.1368	0.15	2.61E−4	1.91E−3

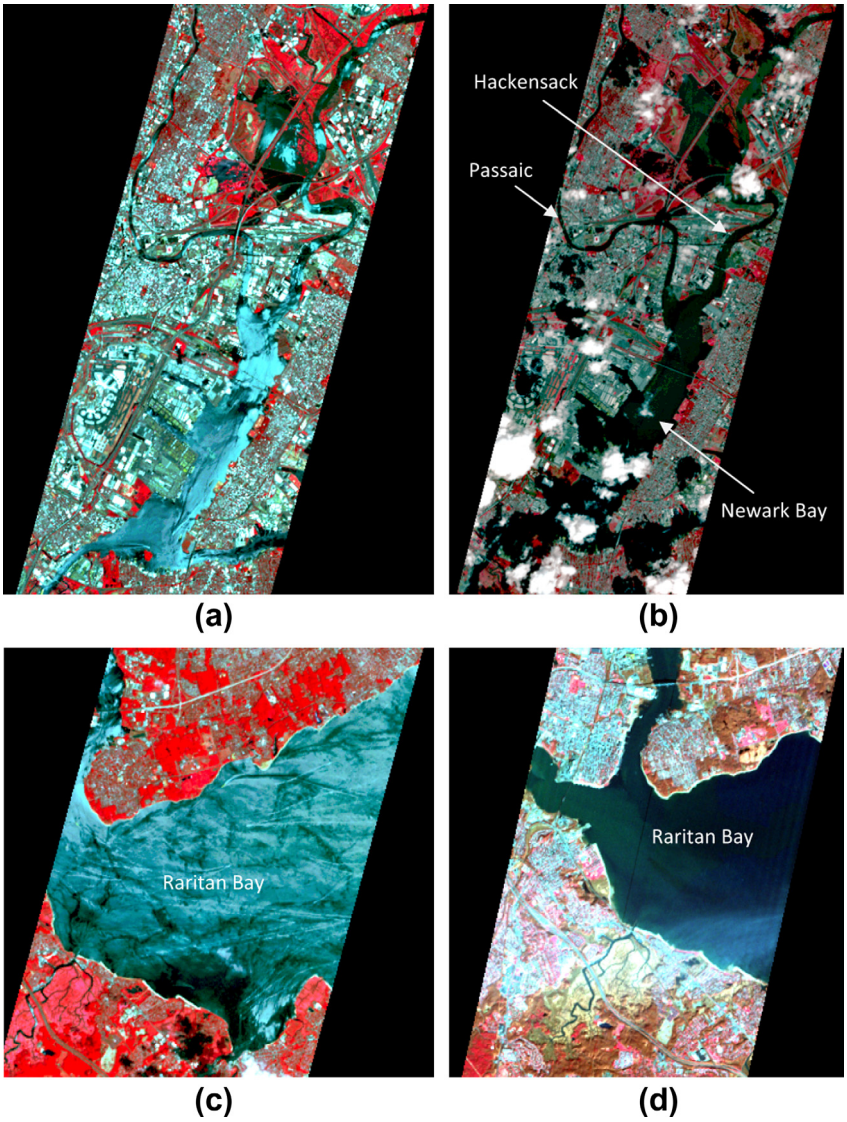

Fig. 4. EO-1 Hyperion images acquired in Hudson site. (a) Hackensack River, Passaic River, and Newark Bay, 07/31/2010, with wind speed 6.8 MPH, sun azimuth 134, sun zenith 61, viewing angle 19. (b) The same area as in (a) but acquired in 10/06/2010, with wind speed 7.9 MPH, sun azimuth 155, sun zenith 41, viewing angle 11. (c) Raritan Bay, 07/31/2010. (d) Raritan Bay, 12/03/2006, wind speed 6.6 MPH, sun azimuth 158.4, sun zenith 24.2, viewing angle −8.8. Most of water surface in the image 07/31/2010 illustrates not only much higher reflectance but also a more chaotic pattern than those in other two images.

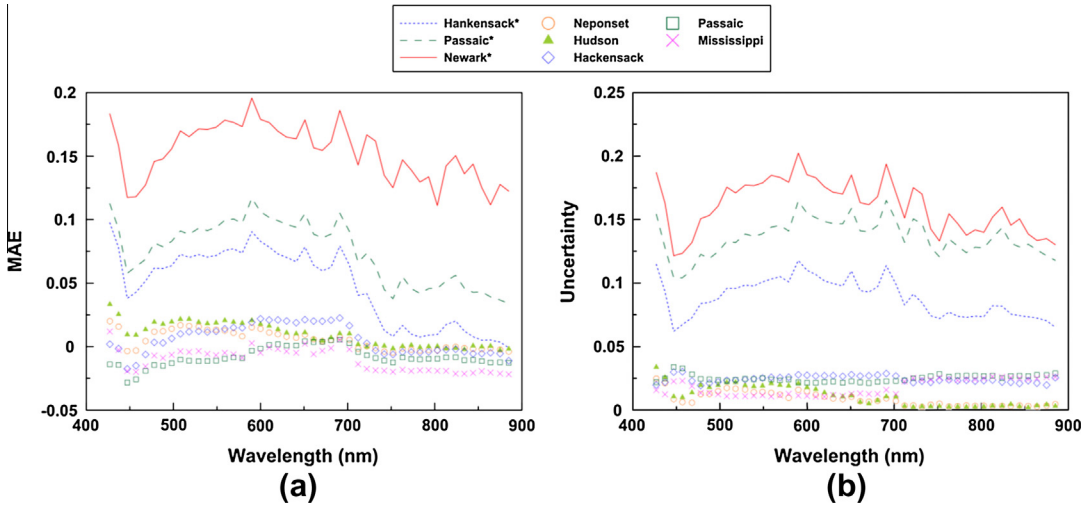

Fig. 5. (a) Mean absolute error (MAE) and (b) uncertainty in level 4, calculated by comparisons between the ASD measured and Hyperion measured spectra (after atmospheric correction). The curves plotted in lines (river names marked by ∗) correspond to those pixels with very high reflectance (surface waves).

4.2. Uncertainties of satellite images

In ocean color remote sensing, water's remote sensing reflectance R_{rs} is the primary information serving for algorithm inversion. When it is fed into algorithms, uncertainties contained in R_{rs} will propagate into all intermediate variables as well as the final results. In this study, R_{rs} is the only input data required by QAA-CDOM, so firstly we need to examine the uncertainties carried by R_{rs}, which is defined by:

$$R_{rs} = \frac{L_w}{E_d} \tag{8}$$

where L_w is water-leaving radiance and E_d is the downwelling spectral plane irradiance incident onto the water surface. E_d is able to be directly measured (in this study, E_d was derived by using either ASD FieldSpec over a reference panel or directly measured by OceanOptics Jaz with a cosine receptor) or simulated by some models like MODTRAN. However, the difficulty of directly measuring L_w impedes calculating R_{rs} from these two measures. We have to estimate L_w from the sensor-received signal by removing the impact of other non-water-leaving factors, such as the radiances contributed by atmosphere, sun glint, sky glint, and whitecaps. The atmospheric path radiance can be removed by atmospheric correction. Based on simulating atmospheric states, a number of atmospheric correction schemes have been developed for retrieving R_t. Here R_t is the total water reflectance which consists of the portion contributed by water surface and the portion contributed by water column. Comparisons and evaluations of these schemes also have been reported by former studies (Anderson et al., 2002; Bulgarelli and Zibordi, 2003; Cairns et al., 2003; Gao et al., 2000). Some schemes aiming to correct surface interference have also been proposed and reviewed (Kay et al., 2009; Mobley, 1999), but they may not be suitable for estuarine regions or efficient for high resolution images. This section we will show some new scenarios of surface states of complex water seen from Hyperion images. And these scenarios may bring large uncertainties into inverse model (level 5).

In this study, the uncertainties and errors of R_t were calculated by comparing the derived R_t from Hyperion (after atmospheric correction using ENVI's FLAASH) and the measured R_t by ASD, which are taken as the true values of R_t. Because ASD is with a narrow field-of-view and its measurement is very close to water surface, the impacts of atmospheric and some surface factors (e.g., sun glint and whitecaps) are basically negligible. In addition, we excluded those ASD data measured over the waters with obvious waves or whitecaps. Note that both ASD and satellite sensor are unable to avoid the surface radiance (L_r) caused by the sky radiance, the uncertainty of L_r is not included in this study. More discussion of L_r can be referred to (Kay et al., 2009; Mobley, 1999).

The Fig. 4 shows that high resolution satellite images may contain some uncertainties. Fig. 4(a) (Hackensack, Passaic and Newark Bay) and (c) (Raritan Bay) are both from the Hyperion image acquired on July 31, 2010. In this image, water shows a very complex and chaotic pattern, and a very high reflectance. This is different from the general experience observed from remote sensing images that water should be slowly varied and dark. The abnormal

Table 3
Image preprocessing uncertainty (level 4) using FLAASH. The values marked by star symbols are the results calculated from strong wave areas. The values in the '*Err*' columns multiple 100 are the error percentages. The Err_4 and Err_{49} are the mean value of 4 bands (440, 490, 555, 640 nm) and 49 bands (426–915 nm) of Hyperion sensor.

Location	Err_{49}	Err_4	*Err* (440)	*Err* (490)	*Err* (555)	*Err* (640)	U_{A49}	U_{A4}	U_A (440)	U_A (490)	U_A (555)	U_A (640)
Neponset	0.128	0.654	1.121	0.655	0.482	0.356	0.009	0.014	0.021	0.013	0.014	0.009
Hackensack	0.119	0.303	−0.112	0.149	0.464	0.711	0.024	0.024	0.022	0.021	0.026	0.027
Hackensack*	2.235	3.430	5.550	3.412	2.501	2.528	0.089	0.095	0.093	0.085	0.103	0.098
Passaic	−0.433	−0.418	−0.801	−0.618	−0.286	0.034	0.025	0.024	0.025	0.024	0.024	0.022
Passaic*	3.370	3.760	5.126	3.193	2.982	3.740	0.136	0.135	0.128	0.119	0.144	0.147
Newark*	9.566	8.551	10.237	7.938	7.461	8.568	0.161	0.168	0.163	0.153	0.188	0.170
Hudson	1.579	3.485	5.606	3.212	2.899	2.222	0.011	0.019	0.026	0.018	0.021	0.011
Atchafalaya	−0.219	−0.080	−0.057	−0.153	−0.058	−0.053	0.018	0.012	0.013	0.014	0.011	0.011
Average	0.235	0.789	1.151	0.649	0.700	0.654	0.017	0.019	0.021	0.018	0.019	0.016
Average*	5.057	5.247	6.971	4.848	4.315	4.945	0.128	0.109	0.128	0.119	0.144	0.138

Table 4
Inverse model uncertainty (level 5) using QAA-CDOM and EO-1 Hyperion images at 6 sites.

Location	n	Measured			Derived			U_A	U_{A1}	U_{A2}	R^2	k	Err	Err	Err_{log}	RMSE	$RMSE_{log}$
		Min	Avg	Max	Min	Avg	Max						Mean	Abs mean	Mean		
Neponset	1143	0.57	0.98	1.53	0.09	0.47	1.42	0.0179	0.0183	0.0189	−0.395	0.447	−0.488	0.494	−0.346	0.607	0.426
Hackensack	1849	0.94	1.16	1.43	0.17	1.35	3.01	0.0126	0.0109	0.0256	0.049	1.162	0.171	0.382	0.027	0.540	0.217
Hudson	3857	0.41	0.75	0.87	0.13	0.28	0.68	0.0077	0.0103	0.0167	0.098	0.374	−0.624	0.625	−0.439	0.479	0.453
Passaic	547	1.01	1.28	1.42	0.58	1.06	1.96	0.0156	0.0121	0.0403	−0.086	0.824	−0.168	0.268	−0.096	0.386	0.152
Atchafalaya	2550	2.60	2.67	2.70	2.17	3.29	4.98	0.0177	0.0066	0.1733	0.013	1.231	0.230	0.255	0.082	0.896	0.117
Newark	592	0.75	0.80	0.87	0.72	1.14	1.95	0.0172	0.0215	0.1424	0.054	1.432	0.430	0.435	0.146	0.419	0.171
All	10,538	0.41	1.34	2.70	0.09	1.31	4.98	0.0061	0.0046	0.0026	0.77	1.102	−0.180	0.450	−0.171	0.622	0.330
Average	1756	1.05	1.27	1.47	0.64	1.27	2.33	0.0148	0.0133	0.0695	−0.045	0.911	−0.075	0.410	−0.104	0.555	0.256

reflectance can be seen by comparing them with the images which cover the same regions but were acquired at different dates. In Fig. 4(b) (10/06/2010) and (d) (12/03/2006), water reflectance is relatively low and there are no any abnormal patterns. The sun glint reflected by surface waves caused these high-value pixels. The local and irregular wind probably is the major factor that makes these waves. In addition, the river's depth, shape, and topography around are all related factors that modulate the waves. Here we do not intend to explore the exact reasons of these waves; instead, we would like to evaluate the reflectance uncertainties made by them.

The results (Fig. 5 and Table 3) show that surface waves significantly magnified the errors and uncertainties of R_t. For each site, about 10 samples were used and samples were obtained with some spatial intervals. For non-wave waters, the average error over 49 visible bands is around 23.5%, and for the 4 bands used by QAA-CDOM, the error is about 78.9%. Among the 4 bands, the error in 440 nm is relatively larger than the others. In general, the errors are significant even for non-wave measurements. Comparatively, the errors and uncertainties produced by waves are always about 5–10 times of the non-waves (7–8 times of the ASD truth). The quality of R_t with so large uncertainty prohibited the image being used for remote sensing inversion.

Although the effects of wind-driven waves can be partly corrected or avoided if we know the wind speed and solar-viewing geometry, for a specific satellite image, it needs to assume that wind speed is a constant through the image scene. This assumption is valid for open seas. However, for riverine and estuarine waters, local irregular winds are difficult to monitor or simulate. An alternative way of glint correction is assuming signal from near-infrared bands should be zero if no glint effect, but unfortunately this assumption is not applicable to shallow and turbid riverine and estuarine water. Whitecap from waves and boats is another factor

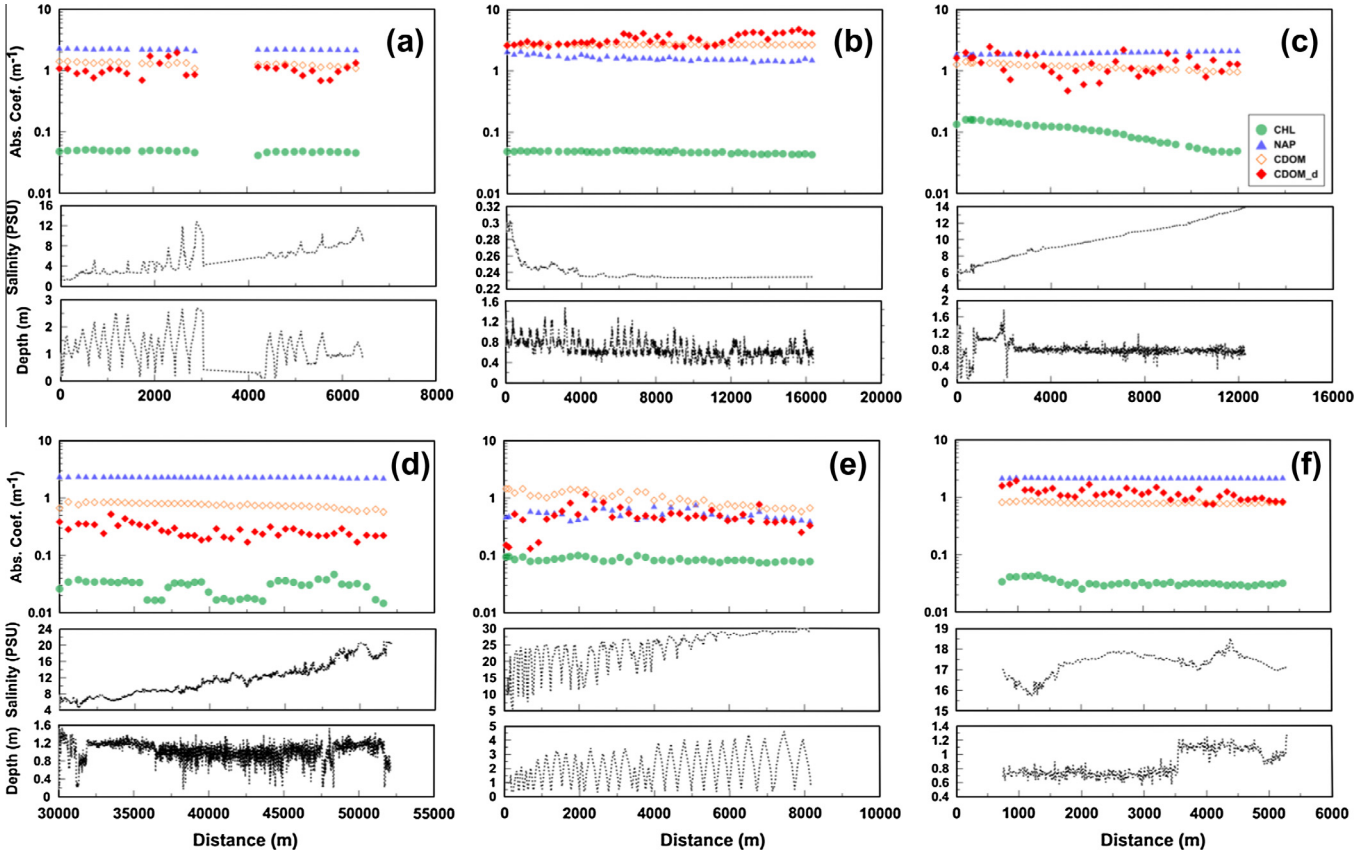

Fig. 6. $a_g(440)$ derived from Hyperion images vs. the measured water properties and depth: (a) Passaic, (b) Atchafalaya, (c) Hackensack, (d) Hudson, (e) Neponset, and (f) Newark. $CDOM_D$ in legends means QAA-CDOM derived $a_g(440)$. The x axis refers to a distance from start point to sampling location along the cruise track (image). Refer to Fig. 2 for start and end points for each site.

contributing to high surface reflectance. They often present in high resolutions images, especially the areas with busy sailing activities, such as the Hudson estuary, Newark Bay, and Boston Bay.

Therefore, based on the results, satellite images with high waves contain large uncertainties if surface reflectance is not properly removed from water-leaving reflectance. The improvement of atmospheric correction and surface reflectance removal schemes may decrease the uncertainty generated by water surface, but cannot solve this problem completely due to the lack of detailed meteorological data at high resolution images level. This large uncertainty suggests avoiding using the Hyperion images with strong sun glint.

4.3. Uncertainties of inversion model

Four Hyperion images with 6 sites, where the Atchafalaya, Hudson, Neponset are from their respective images, and Hackensack, Passaic and Newark Bay are from the same image in 10/06/2010 for minimum glint, were used for uncertainty analysis of inversion model. Statistical and uncertainty variables were calculated and listed in Table 4. Derived and measured CDOM absorption, as well as the measured CHL, NAP, depth, and salinity, along cruise tracks at the 6 sites were plotted in the Fig. 6. For comparison, we only display the data that are both available for in situ ASD and satellite measurements. Due to the high-resolution field measurements, each site contains a large amount (~500–3800) of in situ data. Among the six sites, U_A is around 0.0126–0.0179 with mean 0.0148, but it in the Hudson river is relatively lower (0.0066) due to the large sample size (3857); the U_{A1} in the Atchafalaya river is relatively lower due to the large mean value (2.67), but its U_{A2} is relatively higher due to the narrower range (2.60–2.70). These results indicate that the sample sizes, mean values and ranges all have potential impacts on the evaluations of level-5 uncertainty in different aspects.

The inverted results show that QAA-CDOM performances well with accuracy ($Err_{log} = -0.171$). The average of derived $a_g(440)$ is 1.31, as a comparison to the average of measured $a_g(440) = 1.34$, giving an error percentage of 2.24%. The errors from QAA-CDOM algorithm are positive in Hackensack, Atchafalaya and Newark (Err_{log} are 0.027, 0.082 and 0.146), and negative in Neponset, Hudson and Passaic (Err_{log} are −0.346, −0.439 and −0.096). Overall, The $RMSE_{log} = 0.33$ is close to the result of inversion using ASD data in early research ($RMSE_{log} \sim 0.3$, (Zhu et al., 2011)). For each site, the correlations between the derived and the measured $a_g(440)$ were calculated and indicated by R^2 (regression, Type II) and slope k (the intercept b was set 0). The results show that for each site, the correlations are not significant but slopes are generally good. In Hudson, Neponset and Passaic, $k < 1$ indicates $a_g(440)$ were underestimated and in the other three sites, $a_g(440)$ were overestimated. For the whole six sites, $R^2 = 0.77$ and $k = 1.1$, with $b = 0$, indicating QAA-CDOM performs very well (Fig. 7).

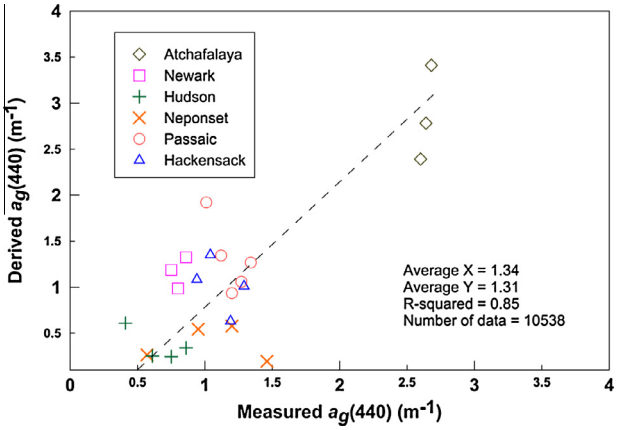

Fig. 7. QAA-CDOM derived vs. the Shuttle measured $a_g(440)$ in six study sites. The number of data point used is 10,538, but they are displayed by randomly resampled. For all data, $R^2 = 0.77$ and $k = 1.1$ with $b = 0$.

The inverse uncertainty is subject to the effect of other water color components, including chlorophyll and non-algal particles; meanwhile, it is associated with other water properties or measurement variables. The correlations between the errors (including AEP) and five variables (CHL, OBS, CDOM, depth, and salinity) were calculated in Table 5. The results show that there is no single variable that is always highly correlated to inverse errors for all sites. The CHL are better correlated in the Neponset and Atchafalaya, but least significant in the Hudson site. The OBS are better correlated in the Hudson, Passaic, and Atchafalaya, but less in the others. The CDOM itself also shows some correlations with the inverse uncertainty. For example, the correlation coefficient 0.82 in the Neponset indicates that the higher CDOM concentrations tend to induce larger errors. The sampling depths have not been seen significantly correlated with inverse uncertainties. This implies that different estuarine systems maintain a unique relationship between CDOM and depth. This leads to the difficulty to infer CDOM at certain depth from the cumulative CDOM absorption captured by remote sensing image. The correlations between salinity and errors are similar to those of between CDOM and errors, since it is known that CDOM correlates to salinity in estuarine and coastal regions due to the dilution of seawater. All above results imply that in some cases chlorophyll is probably the most important and OBS is the second important factor which brings the uncertainties into the CDOM remote sensing inversion because they are both ocean color components that affects underwater light field.

The Type A uncertainties at level 1, 4, and 5 were compared in the Fig. 8. So far there are no evidences indicating that larger uncertainties in low levels will positively propagate to higher levels for certain. For example, in the Neponset, Hudson and Atchafalaya River, the uncertainties of in situ CDOM (level 1) are relatively larger, but compared with other sites, the uncertainties of their

Table 5
Correlation coefficients between five factors (CHL, OBS, CDOM, depth, Salinity) and two errors (error and absolute error percentage).

	Error vs.					Absolute error percentage vs.				
	CHL	OBS	CDOM	Depth	Salinity	CHL	OBS	CDOM	Depth	Salinity
Neponset	0.650	0.148	0.817	0.523	0.802	0.423	0.207	0.587	0.370	0.571
Hackensack	0.055	0.089	0.020	0.017	0.032	0.045	0.055	0.032	0.118	0.045
Hudson	0.032	0.505	0.574	0.084	0.536	0.126	0.138	0.095	0.138	0.063
Passaic	0.000	0.465	0.330	0.095	0.310	0.032	0.000	0.155	0.077	0.182
Atchafalaya	0.609	0.538	0.179	0.281	0.346	0.636	0.559	0.197	0.288	0.327
Newark	0.395	0.292	0.164	0.467	0.190	0.354	0.270	0.110	0.459	0.138
Average	0.399	0.382	0.440	0.313	0.444	0.348	0.274	0.268	0.279	0.286
All	0.089	0.427	0.610	0.316	0.430	0.155	0.401	0.499	0.071	0.307

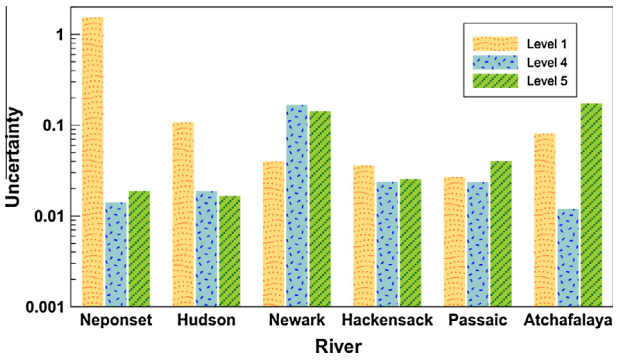

Fig. 8. Uncertainty comparisons in level 1, 4, and 5 in 6 study sites.

remote sensing observations (level 4) are not correspondingly increased. This is because CDOM only contributes a small fraction to the remote sensed signals, and the whole information received by satellite sensors are prone to be affected by other factors, such as sediments, surface waves, and atmosphere. The results show that, except in the Atchafalaya River, there are some correlations between level 4 and level 5 uncertainties in the other 5 sites. This indicates that for a remote sensing inverse model like QAA-CDOM, the input data of high uncertainty will produce a highly uncertain output. The inverted results in the Atchafalaya River indicates that even the input data is with low uncertainty, the output uncertainty is still possible to be high. This implies that the complexity of water itself, for example, the high concentrations of chlorophyll and sediments, as well as the uncertainty of inverse model, will be the major sources of uncertainties of the final results. For water in these cases, we need to further explore the characteristics of its inherent properties and optimize inverse models.

5. Conclusions

In this study the uncertainties involved in the progress of CDOM remote sensing inversion were analyzed. We classified them to 5 levels and focused on the level 1, 4, and 5. Our study sites locate on three estuarine and coastal regions (Mississippi, Hudson, and Neponset) in the North America. The level 1 uncertainty is the uncertainty of in situ CDOM measurement. Based on high resolution in situ data, the uncertainty of field CDOM actually can be represented as the significant digits of a specific measurement, that is, if in the unit of fluorescence (QSU), the uncertainty is around 0.1, and if in the unit of absorption coefficient (m^{-1}), the uncertainty is around 0.01. The normalized CDOM measurement uncertainty is 0.26%. There are no significant differences in level 1 uncertainty for different study sites.

The level 4 uncertainty is related to the satellite remote sensing and image preprocessing (atmospheric correction). We mainly focused on the uncertainty caused by surface waves, which has never been fully investigated before in CDOM remote sensing inversion. The results show that uncertainty of non-wave reflectance is about 0.8 times of the ground truth, while the surface wave reflectance is much larger than the non-wave (about 10 times of the truth). There are no significant differences in level 4 uncertainty for different study sites.

As the level 5 uncertainty, the QAA-CDOM output in the six study sites show that although it may over- or underestimate $a_g(440)$ in each individual site, overall, its accuracy is very excellent (the error for all average value is 2.24% and $RMSE_{log}$ is 0.33). The correlations between uncertainties and other water properties were analyzed. The results indicate that for some rivers, such as the Neponset and Atchafalaya, their relatively large uncertainties are possibly caused by the high concentrations of chlorophyll or sediments. The relationship among the three level uncertainties shows that level 1 uncertainties generally do not propagate into level 4 and 5, but the large uncertainties in level 4 often introduce the corresponding large uncertainties in level 5. In the other side, smaller level 4 uncertainties (e.g. Atchafalaya River) do not always consequently cause smaller uncertainties in level 5. The complexity of water itself and uncertainty of inverse model also have some impacts on the final derived results.

Acknowledgements

This study is supported by a University of Massachusetts Amherst FRG Grant (21644, PI: Q. Yu), an Office of Naval Research Grant (N000140910346, PI: R.F. Chen), a collaborative NSF Grant (1025547, PI: Q. Yu; 1025546, PI: Y.Q. Tian), and a USGS Water Resources Annual Institute Program (2010MA231B, PI: Q. Yu and W.N. Zhu). We would like to thank Robert F. Chen and G. Bernard Gardner for their help and suggestions, as well as all graduate students and staffs who worked in field sample collection and analysis.

References

Anderson, G.P., Felde, G.W., Hoke, M.L., Ratkowski, A.J., Cooley, T., Chetwynd, J.H., Gardner, J.A., Alder-Golden, S.M., Matthew, M.W., Berk, A., Bernstein, L.S., Acharya, P.K., Miller, D., Lewis, P., 2002. MODTRAN4-based atmospheric correction algorithm: FLAASH (Fast Line-of-sight Atmospheric Analysis of Spectral Hypercubes). In: Shen, S.S., and Lewis, P.E. (Eds.), Algorithms and Technologies for Multispectral, Hyperspectral, and Ultraspectral Imagery VIII, vol. 4725: Proceedings of the Society of Photo-Optical Instrumentation Engineers (SPIE), pp 65–71.

Antoine, D., d'Ortenzio, F., Hooker, S.B., Becu, G., Gentili, B., Tailliez, D., Scott, A.J., 2008. Assessment of uncertainty in the ocean reflectance determined by three satellite ocean color sensors (MERIS, SeaWiFS and MODIS-A) at an offshore site in the Mediterranean Sea (BOUSSOLE project). Journal of Geophysical Research-Oceans 113 (C7), C07013.

Blough, N.V., Zafiriou, O.C., Bonilla, J., 1993. Optical-absorption spectra of waters from the Orinoco River outflow – terrestrial input of colored organic-matter to the Caribbean. Journal of Geophysical Research-Oceans 98 (C2), 2271–2278.

Brando, V.E., Dekker, A.G., 2003. Satellite hyperspectral remote sensing for estimating estuarine and coastal water quality. IEEE Transactions on Geoscience and Remote Sensing 41, 1378–1387.

Bricaud, A., Babin, M., Morel, A., Claustre, H., 1995. Variability in the chlorophyll-specific absorption-coefficients of natural phytoplankton – analysis and parameterization. Journal of Geophysical Research-Oceans 100 (C7), 13321–13332.

Bukata, R.P., Jerome, J.H., Kondratyev, K.Y., Pozdnyakov, D.V., 1995. Optical Properties and Remote Sensing of Inland and Coastal Waters. CRC Press, New York.

Bulgarelli, B., Zibordi, G., 2003. Remote sensing of ocean colour: accuracy assessment of an approximate atmospheric correction method. International Journal of Remote Sensing 24 (3), 491–509.

Cairns, B., Carlson, B.E., Ying, R.X., Lacis, A.A., Oinas, V., 2003. Atmospheric correction and its application to an analysis of Hyperion data. IEEE Transactions on Geoscience and Remote Sensing 41 (6), 1232–1245.

Carder, K.L., Chen, F.R., Lee, Z.P., Hawes, S.K., Kamykowski, D., 1999. Semianalytic moderate-resolution imaging spectrometer algorithms for chlorophyll a and absorption with bio-optical domains based on nitrate-depletion temperatures. Journal of Geophysical Research-Oceans 104 (C3), 5403–5421.

Chang, G.C., Gould, R.W., 2006. Comparisons of optical properties of the coastal ocean derived from satellite ocean color and in situ measurements. Optics Express 14 (22), 10149–10163.

Chen, R.F., 1999. In situ fluorescence measurements in coastal waters. Organic Geochemistry 30 (6), 397–409.

Chen, R.F., Bissett, P., Coble, P., Conmy, R., Gardner, G.B., Moran, M.A., Wang, X.C., Wells, M.L., Whelan, P., Zepp, R.G., 2004. Chromophoric dissolved organic matter (CDOM) source characterization in the Louisiana Bight. Marine Chemistry 89 (1–4), 257–272.

Chen, R.F., Gardner, G.B., 2004. High-resolution measurements of chromophoric dissolved organic matter in the Mississippi and Atchafalaya River plume regions. Marine Chemistry 89 (1–4), 103–125.

Del Castillo, C.E., Coble, P.G., Morell, J.M., Lopez, J.M., Corredor, J.E., 1999. Analysis of the optical properties of the Orinoco River plume by absorption and fluorescence spectroscopy. Marine Chemistry 66 (1–2), 35–51.

Ferrari, G.M., Dowell, M.D., Grossi, S., Targa, C., 1996. Relationship between the optical properties of chromophoric dissolved organic matter and total concentration of dissolved organic carbon in the southern Baltic Sea region. Marine Chemistry 55 (3–4), 299–316.

Gao, B.C., Montes, M.J., Ahmad, Z., Davis, C.O., 2000. Atmospheric correction algorithm for hyperspectral remote sensing of ocean color from space. Applied Optics 39 (6), 887–896.

Gardner, G.B., Chen, R.F., Berry, A., 2005. High-resolution measurements of chromophoric dissolved organic matter (CDOM) in the Neponset River Estuary, Boston Harbor, MA. Marine Chemistry 96 (1–2), 137–154.

Garver, S.A., Siegel, D.A., 1997. Inherent optical property inversion of ocean color spectra and its biogeochemical interpretation 1. Time series from the Sargasso Sea. Journal of Geophysical Research-Oceans 102 (C8), 18607–18625.

Huang, W., Chen, R.F., 2009. Sources and transformations of chromophoric dissolved organic matter in the Neponset River Watershed. Journal of Geophysical Research-Biogeosciences 114, G00F05.

IOCCG, 2006. Remote sensing of inherent optical properties: fundamentals, tests of algorithms, and applications. In: Lee, Z.P. (Ed.), Reports of the International Ocean-Colour Coordination Group, No. 5, IOCCG, Dartmouth, Canada.

JCGM, 2008. Evaluation of measurement data – Guide to the expression of uncertainty in measurement, <http://www.bipm.org/en/publications/guides/gum.html> (Accessed 10.05.13).

Kay, S., Hedley, J.D., Lavender, S., 2009. Sun glint correction of high and low spatial resolution images of aquatic scenes: a review of methods for visible and near-infrared wavelengths. Remote Sensing 1 (4), 697–730.

Kirk, J.T.O., 1994. Light and Photosynthesis in Aquatic Ecosystems, second ed. Cambridge University Press, Cambridge, United Kingdom.

Le, C.F., Li, Y.M., Zha, Y., Sun, D.Y., Yin, B., 2009. Validation of a quasi-analytical algorithm for highly turbid eutrophic water of meiliang bay in Taihu Lake, China. IEEE Transactions on Geoscience and Remote Sensing 47 (8), 2492–2500.

Lee, Z.P., Arnone, R., Hu, C.M., Werdell, P.J., Lubac, B., 2010. Uncertainties of optical parameters and their propagations in an analytical ocean color inversion algorithm. Applied Optics 49 (3), 369–381.

Lee, Z.P., Carder, K.L., 2004. Absorption spectrum of phytoplankton pigments derived from hyperspectral remote-sensing reflectance. Remote Sensing of Environment 89 (3), 361–368.

Lee, Z.P., Carder, K.L., Arnone, R.A., 2002. Deriving inherent optical properties from water color: a multiband quasi-analytical algorithm for optically deep waters. Applied Optics 41 (27), 5755–5772.

Lee, Z.P., Weidemann, A., Kindle, J., Arnone, R., Carder, K.L., Davis, C., 2007. Euphotic zone depth: its derivation and implication to ocean-color remote sensing. Journal of Geophysical Research-Oceans 112, C03009.

Melin, F., 2010. Global distribution of the random uncertainty associated with satellite-derived Chla. IEEE Geoscience and Remote Sensing Letters 7 (1), 220–224.

Mobley, C.D., 1999. Estimation of the remote-sensing reflectance from above-surface measurements. Applied Optics 38 (36), 7442–7455.

Nelson, N.B., Siegel, D.A., 2002. Chromophoric DOM in open ocean. In: Hansell, D.A., Carlson, C.A. (Eds.), Biochemistry of Marine Dissolved Organic Matter. Academic Press, San Diego, CA, pp. 547–578.

Nelson, N.B., Siegel, D.A., Carlson, C.A., Swan, C.M., 2010. Tracing global biogeochemical cycles and meridional overturning circulation using chromophoric dissolved organic matter. Geophysical Research Letters 37, L03610.

O'Reilly, J.E., Maritorena, S., Mitchell, B.G., Siegel, D.A., Carder, K.L., Garver, S.A., Kahru, M., McClain, C., 1998. Ocean color chlorophyll algorithms for SeaWiFS. Journal of Geophysical Research-Oceans 103 (C11), 24937–24953.

Ortega-Retuerta, E., Siegel, D.A., Nelson, N.B., Duarte, C.M., Reche, I., 2010. Observations of chromophoric dissolved and detrital organic matter distribution using remote sensing in the Southern Ocean: validation, dynamics and regulation. Journal of Marine Systems 82 (4), 295–303.

Sathyendranath, S., Hoge, F.E., Platt, T., Swift, R.N., 1994. Detection of phytoplankton pigments from ocean color – improved algorithms. Applied Optics 33 (6), 1081–1089.

Siegel, D.A., Maritorena, S., Nelson, N.B., Hansell, D.A., Lorenzi-Kayser, M., 2002. Global distribution and dynamics of colored dissolved and detrital organic materials. Journal of Geophysical Research-Oceans 107 (C12), 3228.

Stedmon, C.A., Markager, S., Sondergaard, M., Vang, T., Laubel, A., Borch, N.H., Windelin, A., 2006. Dissolved organic matter (DOM) export to a temperate estuary: seasonal variations and implications of land use. Estuaries and Coasts 29 (3), 388–400.

Vodacek, A., Blough, N.V., DeGrandpre, M.D., Peltzer, E.T., Nelson, R.K., 1997. Seasonal variation of CDOM and DOC in the Middle Atlantic Bight: terrestrial inputs and photooxidation. Limnology and Oceanography 42 (4), 674–686.

Wang, P., Boss, E.S., Roesler, C., 2005. Uncertainties of inherent optical properties obtained from semianalytical inversions of ocean color. Applied Optics 44 (19), 4074–4085.

Yu, Q., Tian, Y.Q., Chen, R.F., Liu, A., Gardner, G.B., Zhu, W.N., 2010. Functional linear analysis of in situ hyperspectral data for assessing CDOM in Rivers. Photogrammetric Engineering and Remote Sensing 76 (10), 1147–1158.

Zhan, H.G., Shi, P., Chen, C.Q., 2005. A Bayesian based quasi-analytical algorithm for retrieved of inherent optical properties from ocean color. Chinese Science Bulletin 50 (23), 2770–2777.

Zhu, W.N., Tian, Y.Q., Yu, Q., Becker, B., 2013. Using hyperion imagery to monitor the spatial and temporal distribution of colored dissolved organic matter in estuarine and coastal regions. Remote Sensing of Environment 134, 342–354.

Zhu, W.N., Yu, Q., 2013. Inversion of chromophoric Dissolved Organic matter (CDOM) from EO-1 hyperion imagery for turbid estuarine and coastal waters. IEEE Transactions of Geoscience and Remote Sensing 51 (6), 3286–3298.

Zhu, W.N., Yu, Q., Tian, Y.Q., Chen, R.F., Gardner, G.B., 2011. Estimation of chromophoric dissolved organic matter in the Mississippi and Atchafalaya river plume regions using above-surface hyperspectral remote sensing. Journal of Geophysical Research-Oceans 116, C02011.